

Organ-specific dose coefficients derived from Monte Carlo simulations for historical (1930s to 1960s) fluoroscopic and radiographic examinations of tuberculosis patients

David Borrego^{1,5} , A Iulian Apostoaei² , Brian A Thomas² , F Owen Hoffman², Steven L Simon³, Lydia B Zablotska⁴  and Choonsik Lee¹

¹Radiation Epidemiology Branch, Division of Cancer Epidemiology and Genetics, National Cancer Institute, National Institutes of Health, 9609 Medical Center Drive, Bethesda MD 20892-9778, United States of America

²Oak Ridge Center for Risk Analysis, 102 Donner Drive, Oak Ridge TN 37830, United States of America

³Epidemiology and Biostatistics Program, Division of Cancer Epidemiology and Genetics, National Cancer Institute National Institutes of Health, 9609 Medical Center Drive, Bethesda MD 20892-9778, United States of America

⁴Department of Epidemiology and Biostatistics, School of Medicine, University of California San Francisco, San Francisco, CA, 94143-1228, United States of America

E-mail: david.borrego@nih.gov

Received 29 April 2019, revised 26 June 2019

Accepted for publication 3 July 2019

Published 28 August 2019



CrossMark

Abstract

This work provides dose coefficients necessary to reconstruct doses used in epidemiological studies of tuberculosis patients treated from the 1930s through the 1960s, who were exposed to diagnostic imaging while undergoing treatment. We made use of averaged imaging parameters from measurement data, physician interviews, and available literature of the Canadian Fluoroscopy Cohort Study and, on occasion, from a similar study of tuberculosis patients from Massachusetts, United States, treated between 1925 and 1954. We used computational phantoms of the human anatomy and Monte Carlo radiation transport methods to compute dose coefficients that relate dose in air, at a point 20 cm away from the source, to absorbed dose in 58 organs. We selected five male and five female phantoms, based on the mean height and weight of Canadian tuberculosis

⁵ Author to whom any correspondence should be addressed.

patients in that era, for the 1-, 5-, 10-, 15-year old and adult ages. Using high-performance computers at the National Institutes of Health, we simulated 2,400 unique fluoroscopic and radiographic exposures by varying x-ray beam quality, field size, field shuttering, imaged anatomy, phantom orientation, and computational phantom. Compared with previous dose coefficients reported for this population, our dosimetry system uses improved anatomical phantoms constructed from computed tomography imaging datasets. The new set of dose coefficients includes tissues that were not previously assessed, in particular, for tissues outside the x-ray field or for pediatric patients. In addition, we provide dose coefficients for radiography and for fluoroscopic procedures not previously assessed in the dosimetry of this cohort (i.e. pneumoperitoneum and chest aspirations). These new dose coefficients would allow a comprehensive assessment of exposures in the cohort. In addition to providing newly derived dose coefficients, we believe the automation and methods developed to complete these dosimetry calculations are generalizable and can be applied to other epidemiological studies interested in an exposure assessment from medical x-ray imaging. These epidemiological studies provide important data for assessing health risks of radiation exposure to help inform the current system of radiological protection and efforts to optimize the use of radiation in medical studies.

Supplementary material for this article is available [online](#)

Keywords: medical diagnostic exposure, radiation dosimetry, epidemiology, x-rays, fluoroscopy

(Some figures may appear in colour only in the online journal)

1. Introduction

Epidemiological studies of medical exposures of patients provide important data for assessing health risks of radiation exposure. A large cohort of individuals exposed to medical diagnostic and therapeutic procedures includes pulmonary tuberculosis patients treated in Canada in the early 1930s through the 1960s, before chemotherapy was adopted. During that time period, pulmonary tuberculosis was commonly treated by collapsing the diseased lung using pneumothorax or pneumoperitoneum procedures. Induction of a pneumothorax and/or pneumoperitoneum was performed by injecting air or oxygen into the pleural cavity or the peritoneal cavity, respectively (Allen 1941), and fluoroscopy was used to determine the degree of lung collapse and to identify any buildup of fluid around the lung, a potential complication of the treatment. When necessary, chest aspirations were performed to remove the built-up fluid by inserting a needle into the pleural cavity. Throughout the course of treatment for tuberculosis, a patient may have received up to a few hundred fluoroscopies and/or chest radiographs protracted over a period of months to years. In 1965, Steinitz first reported an excess mortality from pulmonary cancer among male tuberculosis patients and, in the following months, Mackenzie, after reporting an observed association between the number of fluoroscopies and breast cancer, hypothesised that the irradiation received during the course of treatment for tuberculosis may have contributed to carcinogenesis (Mackenzie 1965, Steinitz 1965). Subsequent investigators, with more frequent follow-up, reported an elevated incidence of breast

cancer among a population of tuberculosis patients treated in the sanatoria of Nova Scotia (Myrden and Hiltz 1969) and Ontario (Cook *et al* 1974), Canada.

To better study this population of patients and the associated health risks from multiple fluoroscopies, a nationwide epidemiological study, the Canadian Fluoroscopy Cohort Study (CFCS), was initiated in the 1970s (Newcombe 1975). In a recent re-analysis of the CFCS, a significant increase in the risk of cardiovascular mortality was found, in particular for those exposed at younger ages to fractionated x-ray exposures (Zablotska *et al* 2014). Zablotska *et al* (2014) unexpectedly found an inverse relationship between risk and length of protraction, i.e. the risk was greater for those for whom the same dose was delivered over a longer period of time. These previously unrecognised risks of protracted x-ray examinations and the gap in studies of protracted low- to moderate-dose on adults have prompted new efforts to thoroughly re-analyze the CFCS with an additional 30 years of mortality follow-up (1987–2017) and new incidence follow-up (1969–2017). The CFCS cohort presents a unique opportunity to study the radiation dose response from low-dose and low-LET (Linear Energy Transfer) protracted and fractionated radiation exposures.

In the initial dosimetry for this cohort, (Sherman *et al* 1978, Howe and Yaffe 1992), information on the beam quality, patient orientation, and imaged anatomy was obtained from physician interviews and medical record abstraction to derive dose coefficients relating organ absorbed doses to exposure measurements. For procedures that induced pneumothorax, dose coefficients for the breast, thyroid, stomach, liver, ovaries, and active bone marrow were derived by exposing an adult male Alderson-Rando phantom, with a custom breast attachment, and measuring the radiation energy deposited in lithium fluoride (TLD-100) extruded chips placed inside the phantom. For pneumoperitoneum fluoroscopies, however, Monte Carlo radiation transport techniques combined an adult computational human phantom, the ORNL Mathematical Phantom, to calculate dose coefficients (Rosenstein 1976, Sherman *et al* 1978, Cristy and Eckerman 1987, Rosenstein 1988). All dose coefficients for the lung were calculated using Monte Carlo simulations (Kereiakes and Rosenstein 1980, Howe and Yaffe 1992). The measurements of exposure from x-rays at the entrance surface of the skin were taken from the data reported by Boice *et al* (1978), a similar study of tuberculosis patients from Massachusetts, United States, treated between 1925 and 1954. The cumulative organ absorbed dose was then estimated from the total number of fluoroscopic examinations, as indicated by medical records, received by a patient to induce an artificial pneumothorax as part of their treatment regimen. Although sophisticated Monte Carlo radiation transport and dose measurement techniques were adopted in the earlier studies, there were some limitations in those calculations. First, the anatomy of the early adult stylised computational phantom was too simplified to realistically represent the anatomy of adult or pediatric patients (about 18% of the exposed patients were under 20 years of age). Second, the exposure assessment neglected contributions to dose from still-film radiographs and did not make use of appropriate dose coefficients for those procedures. Finally, sensitivity of organ dose computations to different assumptions of imaging parameters were not thoroughly analyzed. Importantly, doses from fluoroscopies associated with pneumoperitoneum or chest aspirations were not included in earlier exposure estimates for the CFCS.

The present study provides improved dose coefficients compared to those used in an earlier exposure assessment of the CFCS patients (28,000 + patients received fluoroscopies and 60,000 + received chest radiographs). The main advancement was in using the latest series of computational human phantoms representing pediatric and adult patients to calculate dose coefficients for both fluoroscopy and radiography examinations. In addition, we also evaluated the sensitivity of organ dose coefficients to different assumptions of technical parameters and setup geometries.

2. Materials and methods

In the current study, we used Monte Carlo radiation transport techniques coupled with advanced computational human phantoms to estimate the amount of energy deposited in tissue from either a fluoroscopic examination or radiograph. To perform individualised dosimetry of a single examination, the following information is required: an understanding of the specific part of the anatomy that was imaged, patient orientation, x-ray beam quality, the distance of the x-ray source to the surface of the patient, and information on the patient such as sex, age, and body morphometry. One of the main challenges in performing a retrospective dose assessment for a large cohort of patients, e.g. the CFCS cohort, is that available medical records do not include all the parameters needed for individualised dose estimation. An additional challenge is the computational time and human resources needed to complete the necessary calculations.

Because of the size of the cohort and the absence of individual exposure data, we developed an approach for dose estimation based on the concept of a representative body size for each age. Our approach, rather than individualised dosimetry, used averaged imaging parameters of beam quality, patient orientation, and imaged anatomy which were collectively defined from measurement data, physician interviews, and literature. We used those imaging parameters in Monte Carlo simulations of radiation transport coupled with computational human phantoms (Geyer *et al* 2014) to compute dose coefficients for the CFCS. The calculated dose coefficient can be used to estimate absorbed dose to tissues using a measurement, or estimate, of exposure at the entrance surface of the body from incident x-rays. Furthermore, we quantified the variation in dose coefficients when the imaging parameters used in the Monte Carlo simulations deviate from their average values in order to quantify uncertainties in doses for this cohort.

2.1. Imaging parameters for fluoroscopy and radiography

For induced pneumothorax procedures, chest aspirations, and chest radiographs, the imaged anatomy is the lung region while imaging during an induced pneumoperitoneum procedure focused on the upper peritoneal cavity and lower lobes of the lungs. In the province of Nova Scotia, fluoroscopic imaging in the anterior-posterior (AP) direction was most common while physicians in other provinces preferred to image primarily in the posterior-anterior (PA) direction, sparing the breast tissues from undue radiation (Howe and Yaffe 1992). Chest radiographs were routinely performed in the PA direction (Kocher *et al* 2019).

The distance between the focal spot and fluoroscopy panel during the 1930s through the 1950s was typically between 30.5 and 33.0 cm. For that reason, we simulated the source-to-skin distance to be 32.5 cm. For radiographs, the common source-to-imaging receptor distance was 182 cm, with the anterior plane of the body facing the imaging receptor, while the source-to-skin distance varied between 155 and 167 cm depending on the computational human phantom thickness.

The open fluoroscopy x-ray field was set to a width of 40.6 cm and a height of 27.9 cm at the fluorescent screen in our simulations (Boice *et al* 1978, Sherman *et al* 1978). For radiographs, we set the field size to a width of 35.6 cm and a height of 43.2 cm at the film cassette (Clark 1939, Rigler 1946, Clark 1949, Clark 1956, Clark 1964). For pediatric patients, the field height was often reduced with the use of vertical shutters so that the same anatomy as for an adult patient (i.e. lung) was imaged. We modeled the use of vertical shutters by collimating the x-ray field in the computations to the smallest field height that encompassed the anatomy of interest. During pneumothorax procedures, left or right shutters were sometimes used to image either the diseased lung, or the opposite lung to check if the disease had spread. For completeness, we also modeled the use of left and right shutters.

Both the combination of imaging procedure and shuttering determine the anatomy of interest and help define the central ray, the portion of the x-ray beam directed towards the center of the imaging receptor. That is, for pneumothorax procedures and chest radiographs, the central ray lies on the mid-sagittal plane, parallel to the transverse plane at a height midway between the apex and base of the lungs. With either left or right shuttering, the central ray is shifted along the horizontal plane to the sagittal plane bisecting the lung of interest. For pneumoperitoneum procedures, the height of the central ray is shifted in the inferior direction so that it lies at the midway point between the middle of the lung and middle of the liver. However, some variation in the position of the central ray is expected, even between examinations of the same patient for the same procedure as a result of small differences in patient orientation. To better understand the effects of this variation, we carried out simulations to model vertical shifts in the central ray location that ranged from 5 cm above to 5 cm below the normal position of the central ray for a typical pneumothorax and pneumoperitoneum procedures. We also estimated the total volume of the organs and tissues that were in-field to better understand the change in dose coefficients due to different beam displacements. Table 1 summarizes x-ray field configurations used in the simulation of fluoroscopy and radiography procedures.

The x-ray source was modeled using 6 beam qualities for fluoroscopies and 12 for radiographs (see table 2). For fluoroscopies, we generated x-ray spectra for applied tube potentials of 50, 75 and 100 kV, a range comparable to those used in medical practice during the 1930s through 1950s (Boice *et al* 1978, Sherman *et al* 1978, Boone and Seibert 1997, Siewerdsen *et al* 2004). In the earliest decades, fluoroscopes were operated with no added filtration, but starting in the early to mid-1940s, filtration equivalent to 1 mm of aluminum was added to remove low energy x-rays. For radiographs, additional x-ray spectra were generated at an applied tube potential of 125 kV and for added filtration equivalent to 1.5 mm of aluminum for all tube potentials (Kocher *et al* 2019).

2.2. Computational human phantoms used to model the human anatomy

To calculate the dose coefficients for the CFCS study, we used a selection of adult and pediatric computational phantoms from a comprehensive library developed in a joint effort between the University of Florida and the National Cancer Institute (Geyer *et al* 2014). The phantom library was created from the reference size pediatric and adult phantoms (Lee *et al* 2010) by non-uniformly scaling each body part to match body morphometry data collected from 1999–2006 by the National Health and Nutrition Examination Survey (NHANES) IV⁶ of the United States population. For our study, we selected 10 phantoms, 5 of each sex, from the library to represent the patients of ages of 1, 5, 10, 15 years and adult, by closely matching the mean height and weight of tuberculosis patients treated in Canada from 1930s to 1960s as outlined in table 3 (Thiessen 2017). Using a previously developed method (Lee *et al* 2013), lymphatic nodes were added at 16 cluster locations based on the recommendations from the ICRP Publications 23 and 89. We updated the heart model, previously consisting of left and right chambers only, using patient imaging datasets with nine cardiac structures contoured from contrasted computed tomography images obtained from the National Institutes of Health Clinical Center. The heart model, as shown in figure 1, now includes 9 structures: aorta, left main coronary artery, left atrium, left anterior descending artery, left circumflex artery, left ventricle, right atrium, right coronary artery, and right ventricle. In total, we calculated the energy deposition for 58 (female) and 57 (male) organs and tissues which include the breast, lung, heart, and active bone marrow.

⁶ <https://www.cdc.gov/nchs/nhanes/index.htm>

Table 1. X-ray field configurations used in simulations of treatment of tuberculosis from 1930s to 1960s.

	Pneumothorax using shuttering			Pneumoperitoneum using shuttering		Radiographs
	Open	Vertical	Left/Right	Open	Vertical	
Central ray	Open and Vertical: Central ray lies on the mid - sagittal plane and is parallel to the transverse plane.		Central ray lies on the sagittal plane that bisects the lung and is parallel to the transverse plane.	All: Central ray lies on the mid-sagittal plane, parallel to the transverse plane and is centered at the midway point between the middle of the lung and middle of liver.		Central ray points in the posterior-anterior direction, lies on the mid-sagittal plane between the base and apex of the lungs, and is parallel to the transverse plane.
	<small>All: X ray field is centered between the base and apex of the lungs</small>					
X-ray field size	40.6 × 27.9 cm (width × height) at the imaging receptor	Width of field reduced to encompass left or right lung		40.6 × 27.9 cm at the imaging receptor	The top and bottom border bisect the lung and liver	35.6 × 43.2 cm at the imaging receptor
	<small>Vertical, and left/right: The top and bottom border are level with the apex and base of the lungs.</small>					
Variable parameters	Orientation and beam quality	Orientation, beam quality, and central ray vertical position	Orientation and beam quality	Orientation and beam quality	Orientation, beam quality, and central ray vertical position	Beam quality and vertical shuttering ^a

^a Dose coefficients for vertical shuttering were computed and tabulated in the supplementary material; however, public health reports indicated shuttering was not commonly used during chest radiographs before the 1950s.

Table 2. Characteristics of x-ray spectra modeled in the Monte Carlo radiation transport to generate dose coefficients.

Peak tube potential (kV)	Added filtration (mm of Al)	Total filtration (mm of Al)	First HVL ^a (mm of Al)	\bar{E} ^b (keV)
Fluoroscopy				
50	None	0.5	0.66	27
50	1.0	1.5	1.16	30
75	None	0.5	0.85	35
75	1.0	1.5	1.60	38
100	None	0.5	1.12	42
100	1.0	1.5	1.93	45
Radiography				
50	None	0.5	0.65	27
50	1.0	1.5	1.30	30
50	2.0	2.5	1.74	32
75	None	0.5	0.97	35
75	1.0	1.5	1.91	39
75	2.0	2.5	2.55	41
100	None	0.5	1.35	43
100	1.0	1.5	2.57	47
100	2.0	2.5	3.41	49
125	None	0.5	1.81	49
125	1.0	1.5	3.31	53
125	2.0	2.5	4.32	56

^a Half-value layer (HVL) in mm of aluminum (Al) equivalent.

^b \bar{E} is the mean photon energy of the x-ray spectra.

Table 3. Height and weight of computational phantoms selected to match mean height and weight of tuberculosis patients treated in Canada from 1930s to 1960s (Thiessen 2017)^a.

Age	Sex	Canadian TB population		Computational phantom (Geyer <i>et al</i> 2014)	
		Height (cm)	Weight (kg)	Height (cm)	Weight (kg)
1 year	Male	76	9.9	76	10
5 years	Male	106	18.1	105	20
10 years	Male	136	28.6	135	30
15 years	Male	164	48.6	165	50
Adult	Male	170	66.0	170	65
1 year	Female	74	9.4	76	10
5 years	Female	106	18.6	105	20
10 years	Female	135	28.2	135	30
15 years	Female	158	45.7	155	45
Adult	Female	157	55.1	155	55

^a Based on Canadian national survey with adjustments for weight loss due to tuberculosis.

2.3. Reporting of Monte Carlo radiation transport

We used the Monte Carlo N-particle eXtended (MCNPX) transport code version 2.7.1, a code that is well benchmarked for medical radiation dosimetry applications (Pelowitz 2011). For

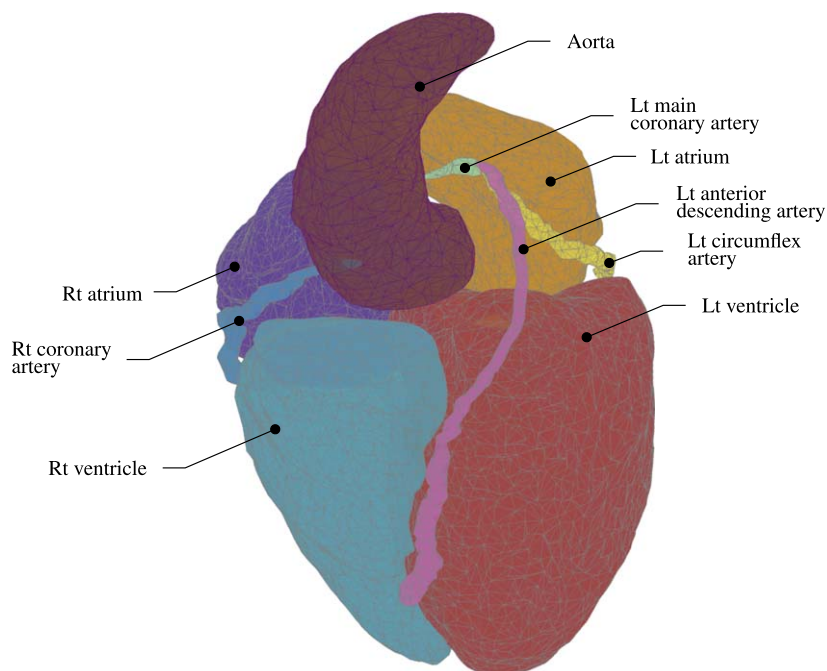


Figure 1. 3D rendering of the detailed cardiac model for male patients developed from contrasted CT images with 9 substructures delineated.

the current study, the radiation source was defined as an anisotropic point source for 1 keV bins increasing up to the peak tube potential. Collimation of the simulated x-ray beam was then introduced with the use of zero importance surfaces, i.e. surfaces that stop transporting all incident particles, to produce a diverging rectangular field. The MCNP code simulated the transport of both photons and electrons using ENDF/B-VII cross section libraries (Pelowitz 2011). The photon physics in the code allowed for the generation of electrons and coherent scattering. All electrons were transported until their energy fell below 1 keV, at which point their energy is assumed to be locally deposited. We calculated energy deposition across all organs and tissues of interest and for a small volume of air, a detector, prior to the entrance surface in order to calculate the dose coefficients. For each simulation, we allowed the radiation transport to run until 500 million particle histories were recorded or until a computational time of 50 hours was reached with no further variance reduction. These computational settings ensured that the relative errors in the calculated energy deposition are less than 1% for all organs in the primary x-ray field.

From the Monte Carlo simulations of radiation transport, the dose coefficient, DC , was derived using equation (1)

$$DC = (ED)_{Detector @ 20 \text{ cm}}^{Tissue} \quad (1)$$

The DC is the quotient of energy deposition, ED , per source starting particle in a tissue of interest to the ED in the detector at a position 20 cm from the x-ray tube and free-in-air. However, the distance between the x-ray tube and measurements of tube output is often performed at the source to skin distance and not at 20 cm as modeled in our simulations. In our simulations we intentionally shifted the detector upstream towards the source to minimize backscattering contributions. The values of DC shown in figures 2–5 have been adjusted to

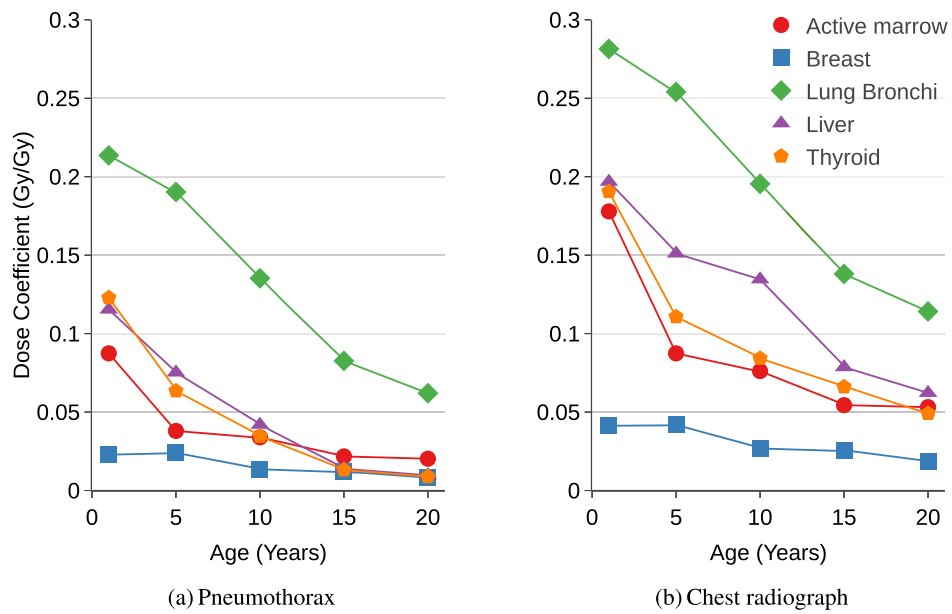


Figure 2. Age-dependent dose coefficients (Gy in tissue/Gy in air) for female patients undergoing (a) pneumothorax procedure and (b) chest radiography performed in the posterior-anterior direction at 75 kV with no added filtration and for an open beam.

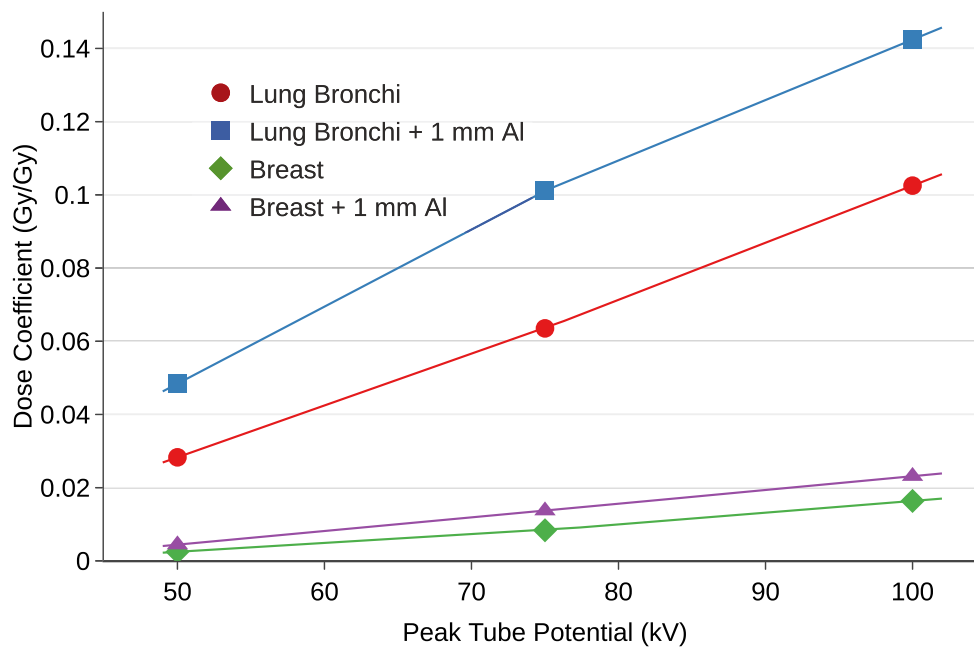


Figure 3. Organ dose coefficients for different peak tube potentials for an adult female undergoing a pneumothorax and imaged in the posterior-anterior direction with and without 1 mm of Al filtration.

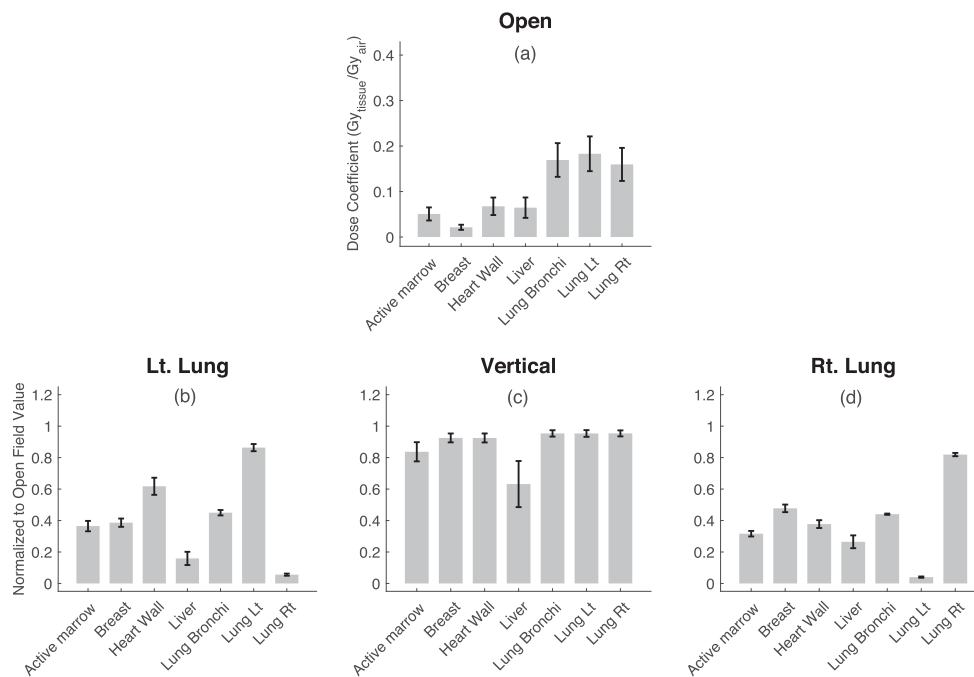


Figure 4. Variability of dose coefficients averaged over energies and ages for fluoroscopy during a posterior-anterior pneumothorax procedure due to different shuttering setups with 95% confidence intervals for four shuttering setups: (a) open, (b) left lung, (c) vertical and (d) right lung shuttering.

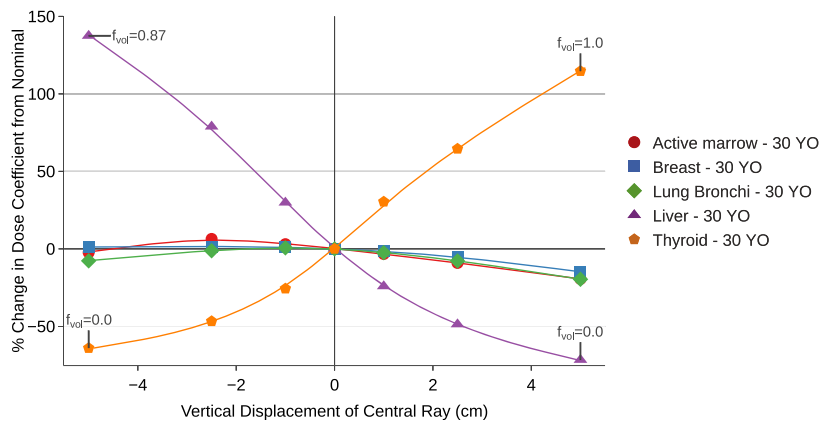


Figure 5. Change in the adult female dose coefficients from its nominal value of a 0 cm displacement in the central ray height. The reported values are for fluoroscopy during a pneumothorax procedure performed in the posterior-anterior direction with vertical shuttering. f_{vol} denotes the fractional volume of the tissue located within the primary x-ray field.

account for the geometric attenuation between the location of the detector modeled in the Monte Carlo simulations and the location of tube output measurements using inverse square law approximation.

3. Results

In total, we performed 2,400 Monte Carlo simulations. This task would have taken over 4.4 years on a single processor PC; however, we utilised the computational resources of the NIH high performance computing center to perform this task, distributed over thousands of processors, in a matter of weeks. The output files were then post-processed with scripts to abstract the data.

The estimated dose coefficients can be grouped according to the age of persons represented by each of the computational human phantom used (1-, 5-, 10-, 15-year-old and adult males and females) (table 1), x-ray beam quality (table 2), imaging modality (fluoroscopy or radiography), procedure type (pneumothorax, pneumoperitoneum, or chest aspiration) (table 3), and the direction of x-rays through the anatomy (AP or PA). A complete table of the dose coefficients and associated relative errors can be found in the supplemental materials (available online at stacks.iop.org/JRP/39/950/mmedia). For brevity in the Discussion section, we focused on dose coefficients for the female to highlight trends in age, beam quality, central ray position, and shuttering. The calculated dose coefficients extend down to the age of 1 year whereas previous dose coefficients for this cohort were limited to tissues of an adult (Sherman *et al* 1978, Howe and Yaffe 1992).

In general, we observed that the dose coefficients decrease with increasing age at exposure; however, this effect is less pronounced for deep-seated organs, as shown in figure 2. Between the female phantoms of 1-year of age and adult, the lung bronchi dose coefficient decreases by a factor of 3.4 and 2.8 for pneumothorax and chest radiography, respectively. Likewise, for the breast, the dose coefficient decreases with increasing age by a factor of 2.5 (pneumothorax) and 2.2 (radiography). If no adjustment in the technique factors (e.g. applied tube potential, tube-current exposure-time product, and/or amount of added filtration) is assumed for pediatric patients that underwent treatment, then it can be expected that the absorbed doses to their organs would be greater than that of adult patients. A similar decrease in dose coefficients with increasing body size was observed when using the PC program for x-ray Monte Carlo (PCXMC), developed by Tapiovaara and Siiskonen (2008), which incorporates a version of the stylised ORNL mathematical phantoms adjustable by body size (Borrego *et al* 2018).

For this study, we quantified the possible range of values in the dose coefficients over 6 beam qualities in fluoroscopy and 12 beam qualities in radiography. Increasing the average energy of the x-ray beam, either through added filtration or an increase in the applied tube potential, increased the dose coefficient, see figure 3. Dose coefficients for the lung bronchi in an adult female at a peak potential of 100 kV are greater than those for 50 kV by up to a factor of 3.0 and 3.7, with and without added filtration, respectively. The hardest fluoroscopy beam (highest average energy), 100 kV and filtered through 1 mm of aluminum (Al), had a 1.93 mm of Al half-value layer. In radiography, the hardest x-ray beam had a half value layer of 4.32 mm of Al with an applied tube potential of 125 kV and filtered through 2 mm of Al.

The variation in dose coefficients (averaged over energies and ages) due to different shuttering positions (open, vertical, left and right lung shuttering) for a pneumothorax procedure performed in the posterior-anterior direction are shown in figure 4(a). The dose coefficients are greatest for the in-field organs such as the lung and heart, the latter being shielded considerably by the body. The dose coefficients for organs near the anatomy of interest are reduced when vertical shutters are used, with little to no reduction in the dose coefficients for the anatomy of interest. For example, applying vertical shutters (figure 4(c)) reduced the liver dose coefficient to 63% of its original value for open shutters (figure 4(a)) whereas, for the in-field organs (e.g. lungs), the dose coefficient remained at 92% or greater of

their original value. When either left or right shuttering was modeled (figures 4(b) and (d)), the dose coefficients of the imaged lung, on average, were reduced to 86% and 82% of their open shutter values, respectively, whereas the dose coefficient of the non-imaged lung is reduced to less than 6% of its open shutter value. The open field size of 40.6 cm width by 27.9 cm height is far too large for the smaller anatomy of a pediatric patient and fully encompasses organs that were near/partially-in-field in the adult patients, such as the liver and for this reason the liver dose coefficients are elevated with the inclusion of pediatric patients, see figure 4(a).

4. Discussion

This work provides dose coefficients necessary to perform a radiation exposure assessment for patients exposed during the course of treatment for tuberculosis in the 1930s through the 1960s. We used advanced computational human phantoms covering adult ages down to pediatric patients 1 year of age to calculate our dose coefficients. Our dose coefficients are sex-specific which was often not the case in previous exposure assessments of this cohort. Moreover, we provide dose coefficients for up to 58 tissue structures including the heart and associated structures, lymph nodes, and active bone marrow, whereas previously only the lung and breast were reported for the CFCS. In addition, we provide dose coefficients for fluoroscopy and radiography procedures. Finally, we considered different imaging parameters which allowed us to quantify the variability in dose coefficients and their sensitivity to imaging parameters that deviate from average values.

For both pneumothorax and pneumoperitoneum procedures we explored sensitivity of the dose coefficient calculations to vertical displacements in the central ray location of up to ± 5 cm from the normal position of the central ray. The percent change in the dose coefficient relative to normal (0 cm displacement in the central ray) was less than 20% for organs that are originally in-field. However, for organs located near the primary x field, i.e. near-field organs, the percent change was found to be substantial. For example, looking at figure 5, when the central ray was shifted in the direction of a near-field organ, the dose coefficient would increase, in excess of 100% — see thyroid values under a positive displacement and liver values under a negative displacement. We added the fraction of organ volume included in the primary x-ray field to the graph. A fractional value of 1 would indicate that the organs are fully contained within the primary x-ray field.

A special research effort was dedicated to estimating typical body weights and heights for Canadian tuberculosis patients during the period from 1930 to 1969. The results of that research (Thiessen 2017) were summarised in two parts: (1) selection or estimation of average heights and weights for the Canadian white population during the time period of interest; and (2) estimation of any difference in body weight between tuberculosis patients and healthy individuals. Most tuberculosis patients experience weight loss due to their disease and they are, on average, thinner than average members of the general population. Our research indicated that the average body weights of tuberculosis patients are about 10% lower than the average body weights for males and females ages 8 and older in the general population. For 6- and 7-year-old males, average body weight in tuberculosis patients is 5% lower compared to body weights of healthy individuals. Younger children (ages <5 for males and ages <7 for females) are expected to have little or no weight loss. While the average body weights and heights of males and females in the general Canadian population are relatively well known, being based on good statistics and large number of samples, the average weight loss and the estimated average body weights in tuberculosis patients are uncertain. The magnitude of

uncertainty in the average weight is on the order of $\pm 6\%$ or less (minimum to maximum range) of the nominal weight by age and sex (Thiessen 2017). Based on several recent studies that report dose coefficients for the purpose of estimating radiation doses from medical exposures (Simon 2011, Borrego *et al* 2018, Chang *et al* 2018), and based on a sensitivity analysis of the dose coefficients derived for this study we expect that the uncertainty in the average organ-specific dose coefficients due to the uncertainty in average body weights for Canadian tuberculosis patients is about $\pm 10\%$ – 20% (minimum to maximum range), with narrower uncertainty ranges possible for some organs.

For pneumothorax procedures, the lung dose coefficients to the adult female are lower than previously reported by factors of 0.6 (open x-ray field at 75 kV with added filtration) to 0.9 (under vertical shuttering and no added filtration) in the posterior-anterior orientation but larger when in the anterior-posterior direction by factors of 1.5 (open x-ray field with added filtration) to 2.3 (no added filtration) (Howe and Yaffe 1992). Our breast dose coefficients are lower than those previously reported in both the posterior-anterior and anterior-posterior directions by factors ranging from 0.36 (posterior-anterior simulation with an open x-ray field at 75 kV with added filtration) to 1.0 (anterior-posterior simulation with no added filtration) (Howe and Armstrong 1993). A complete table comparing our newly calculated lung and breast dose coefficients to previously reported values for this cohort can be found in the supplemental materials. The differences in the dose coefficients are likely due to anatomical differences between the CT imaging-based phantoms used in the current study compared to the previously used ORNL Mathematical Phantom, a simplified stylised phantom. For example, we noticed that for the adult phantoms the lung is located nearer to the anterior surface whereas in the styled phantom used in previous studies the lung is nearer to the posterior surface. Several studies have highlighted improvements in dosimetry with the use of newer phantoms with improved anatomical realism when compared to the stylised phantoms (Kramer *et al* 2008, Park *et al* 2008, Johnson *et al* 2011).

The following limitations are present in our study, in common with other retrospective dosimetry studies. Many of our simulated technique factors are based on physician interviews and/or a review of the medical literature instead of being informed by the medical records of each exposed patient. *In-vivo* dosimetry is not available, nor do we have patient-specific anatomy data or imaging datasets to construct patient specific phantoms. Almost all members of the CFCS cohort would be deceased at this time, making the acquisition of patient-specific data impossible. As such, as is common for these studies, we used anatomical models, derived from normal anatomy, that best represent the average characteristics of height and weight for the exposed population.

5. Summary

The current work provides new dose coefficients for the adult and pediatric populations treated for tuberculosis in the Canadian Fluoroscopy Cohort Study (CFCS). In addition, this work adds dose coefficients for organs and tissues not previously considered, in particular those outside the primary x-ray beam. Furthermore, the new dose coefficients were calculated using the latest computational human phantoms that more realistically resemble the human anatomy, complete with lymphatic nodes and a detailed heart model. These dose coefficients are a first step in revising and providing a comprehensive exposure assessment for the CFCS cohort.

We are making this dataset of dose coefficients openly available. Future use of this dataset may include, for example, the Massachusetts tuberculosis study (Boice and

Monson 1977, Boice *et al* 1978, Boice 1978). Our dose coefficients for chest radiography are for beam qualities too soft for modern day radiography, which is almost always filtered through thicker layers of aluminum and, at times, copper. However, our dose coefficients could be applied to compute organ doses for chest radiographs until the late 20th century, or via extrapolation to the x-ray spectra generated by modern day equipment. We believe the automation and dosimetry methods developed to complete this work are generalizable to other epidemiological studies of radiogenic health risks from exposure to diagnostic x-ray procedures.

Acknowledgments

This work was funded by National Cancer Institute and National Institutes of Health award R01CA197422 through a subcontract to Oak Ridge Center for Risk Analysis, Inc. (AIA, BAT, FOH), from the University of California, San Francisco (Principal Investigator: L B Zablotska). This work utilised the computational resources of the NIH HPC Biowulf Cluster (<http://hpc.nih.gov>).

Financial disclosures

This work was supported by the Intramural Research Program of the National Cancer Institute, National Institutes of Health.

ORCID iDs

David Borrego  <https://orcid.org/0000-0001-9868-5113>
A Iulian Apostoaei  <https://orcid.org/0000-0001-9750-6056>
Brian A Thomas  <https://orcid.org/0000-0003-0384-8966>
Lydia B Zablotska  <https://orcid.org/0000-0002-0778-1108>

References

- Allen L L 1941 Pneumoperitoneum in the treatment of pulmonary tuberculosis *Journal of the National Medical Association* **33** 57–60
- Boice J D 1978 Follow-up methods to trace women treated for pulmonary tuberculosis, 1930–1954 *Am. J. Epidemiol.* **107** 127–39
- Boice J D Jr and Monson R R 1977 Breast cancer in women after repeated fluoroscopic examinations of the chest *J. Natl. Cancer Inst.* **59** 823–32
- Boice J D, Rosenstein M and Trout E D 1978 Estimation of breast doses and breast cancer risk associated with repeated fluoroscopic chest examinations of women with tuberculosis *Radiat. Res.* **73** 373–90
- Boone J M and Seibert J A 1997 An accurate method for computer-generating tungsten anode x-ray spectra from 30 to 140 kV *Med. Phys.* **24** 1661–70
- Borrego D, Lowe E M, Kitahara C M and Lee C 2018 Assessment of PCXMC for patients with different body size in chest and abdominal x-ray examinations: a Monte Carlo simulation study *Phys. Med. Biol.* **63** 065015
- Chang L A, Borrego D and Lee C 2018 Body-weight dependent dose coefficients for adults exposed to idealised external photon fields *J. Radiol. Prot.* **38** 1441–53
- Clark K C 1939 *Positioning in Radiography* 1st edn (London, UK: Ilford Ltd, William Heineman Medical Books)

- Clark K C 1949 *Positioning in Radiography*, 5th edn (revised) (London, UK: Ilford Ltd, William Heineman Medical Books)
- Clark K C 1956 *Positioning in Radiography* 7th edn (revised) (London, UK: Ilford Ltd, William Heineman Medical Books)
- Clark K C 1964 *Positioning in radiography* 8th edn (London, UK: Ilford Ltd, William Heineman Medical Books)
- Cook D C, Dent O and Hewitt D 1974 Breast cancer following multiple chest fluoroscopy: the Ontario experience *Canadian Medical Association Journal* **111** 406–9
- Cristy M and Eckerman K F 1987 *Specific Absorbed Fractions of Energy at Various Ages from Internal Photon Source*. vol ORNL/TM-8381/V1 (Oak Ridge: Oak Ridge National Laboratory)
- Geyer A M, O'Reilly S, Lee C, Long D J and Bolch W E 2014 The UF/NCI family of hybrid computational phantoms representing the current US population of male and female children, adolescents, and adults—application to CT dosimetry *Phys. Med. Biol.* **59** 5225–42
- Howe G R and Armstrong B 1993 The effect of measurement error in doses on risks of radiation induced breast and lung cancers and leukemia *Report* (Ottawa, Ontario: Atomic Energy Control Board) 1–68
- Howe G R and Yaffe M 1992 *Estimation of Lung Tissue Doses following Exposure to Low-LET Radiation in the Canadian Study of Cancer Following multiple Fluoroscopies* (Ottawa, Canada: International Atomic Energy Agency)
- Johnson P B, Geyer A, Borrego D, Ficarrotta K, Johnson K and Bolch W E 2011 The impact of anthropometric patient-phantom matching on organ dose: a hybrid phantom study for fluoroscopy guided interventions *Med. Phys.* **38** 1008–17
- Kereiakes J G and Rosenstein M 1980 *Handbook of Radiation Doses in Nuclear Medicine and Diagnostic X-Ray* (Boca Raton, Florida: CRC Press, Inc.)
- Kocher D C, Apostoaei A I, Thomas B A, Borrego D, Lee C and Zablotska L B 2019 Organ doses from chest radiographs in tuberculosis patients in Canada and their uncertainties in periods from 1930 to 1969 *Health Phys.* (accepted)
- Kramer R, Khoury H J and Vieira J W 2008 CALDose_X—a software tool for the assessment of organ and tissue absorbed doses, effective dose and cancer risks in diagnostic radiology *Phys. Med. Biol.* **53** 6437–59
- Lee C, Lamart S and Moroz B E 2013 Computational lymphatic node models in pediatric and adult hybrid phantoms for radiation dosimetry *Phys. Med. Biol.* **58** N59–82
- Lee C, Lodwick D, Hurtado J, Pafundi D, Williams J L and Bolch W E 2010 The UF family of reference hybrid phantoms for computational radiation dosimetry *Phys. Med. Biol.* **55** 339–63
- Mackenzie I 1965 Breast cancer following multiple fluoroscopies *British Journal of Cancer* **19** 1–8
- Myrden J A and Hiltz J E 1969 Breast cancer following multiple fluoroscopies during artificial pneumothorax treatment of pulmonary tuberculosis *Canadian Medical Association Journal* **100** 1032–4
- Newcombe H B 1975 *Cancer Following Multiple Fluoroscopies* (Ontario: Chalk River)
- Park S H, Lee J K and Lee C 2008 Dose conversion coefficients calculated using tomographic phantom, KTMAN-2, for x-ray examination of cardiac catheterisation *Radiat. Prot. Dosim.* **128** 351–8
- Pelowitz D B 2011 MCNPX users manual version 2.7.0 *Report* LA-CP-11-00438 (Los Alamos, NM: Los Alamos National Laboratory)
- Rigler L G 1946 *The Chest: a Handbook of Roentgen Diagnosis*. (Chicago, IL: The Year Book Publishers)
- Rosenstein M 1988 *Handbook of Selected Tissue Doses for Projections Common in Diagnostic Radiology*. (CDRH Report FDA 89-8031) (MD: Rockville)
- Rosenstein M 1976 *Organ Doses in Diagnostic Radiology* (MD: Rockville)
- Sherman G J, Howe G R, Miller A B and Rosenstein M 1978 Organ dose per unit exposure resulting from fluoroscopy for artificial pneumothorax *Health Phys.* **35** 259–69
- Siewerdsen J H, Waese A M, Moseley D J, Richard S and Jaffray D A 2004 Spektr: a computational tool for x-ray spectral analysis and imaging system optimization *Med. Phys.* **31** 3057–67
- Simon S L 2011 Organ-specific external dose coefficients and protective apron transmission factors for historical dose reconstruction for medical personnel *Health Phys.* **101** 13–27
- Steinitz R 1965 Pulmonary tuberculosis and carcinoma of the lung. A survey from two population-based disease registers *Am. Rev. Respir. Dis.* **92** 758–66
- Tapiovaara M and Siiskonen T 2008 PCXMC. A Monte Carlo program for calculating patient doses in medical x-ray examinations *STUK-A231* (Helsinki: STUK)

- Thiessen K M 2017 *Heights and Body Weights of Canadian Tuberculosis Patients* (Oak Ridge, TN: Oak Ridge Center for Risk Analysis) (https://zablotskaresearchgroup.ucsf.edu/sites/zablotskaresearchgroup.ucsf.edu/files/CFCS%20Body%20Weights%20Heights_Thiessen%202017.pdf)
- Zablotska L B, Little M P and Cornett R J 2014 Potential increased risk of ischemic heart disease mortality with significant dose fractionation in the Canadian fluoroscopy cohort study *Am. J. Epidemiol.* **179** 120–31